Since January 2020 Elsevier has created a COVID-19 resource centre with free information in English and Mandarin on the novel coronavirus COVID-19. The COVID-19 resource centre is hosted on Elsevier Connect, the company's public news and information website.

Biochemical Pharmacology 182 (2020) 114215

Contents lists available at ScienceDirect

Biochemical Pharmacology

journal homepage: www.elsevier.com/locate/biochempharm

The inorganic polymer, polyphosphate, blocks binding of SARS-CoV-2 spike protein to ACE2 receptor at physiological concentrations

Meik Neufurth[a], Xiaohong Wang[a,*], Emad Tolba[a], Ingo Lieberwirth[b], Shunfeng Wang[a], Heinz C. Schröder[a], Werner E.G. Müller[a,*]

[a] ERC Advanced Investigator Grant Research Group at the Institute for Physiological Chemistry, University Medical Center of the Johannes Gutenberg University, Duesbergweg 6, D-55128 Mainz, Germany
[b] Max Planck Institute for Polymer Research, Ackermannweg 10, D-55128 Mainz, Germany

ARTICLE INFO

Keywords:
Polyphosphate
Nanoparticles
SARS-CoV-2 spike S-protein
Binding assay
COVID-19

ABSTRACT

Inorganic polyphosphate (polyP) is a morphogenetically active and metabolic energy-delivering physiological polymer that is released from blood platelets. Here, we show that polyP efficiently inhibits the binding of the envelope spike (S)-protein of the coronavirus SARS-CoV-2, the causative agent of COVID-19, to its host cell receptor ACE2 (angiotensin-converting enzyme 2). To stabilize polyP against the polyP-degrading alkaline phosphatase, the soluble polymer was encapsulated in silica/polyP nanoparticles. Applying a binding assay, soluble Na-polyP (sizes of 40 P_i and of 3 P_i units) as well as silica-nanoparticle-associated polyP significantly inhibit the interaction of the S-protein with ACE2 at a concentration of 1 μg/mL, close to the level present in blood. This inhibition is attributed to an interaction of polyP with a basic amino acid stretch on the surface of the receptor binding domain of S-protein. PolyP retains its activity in a flushing solution, opening a new strategy for the prevention and treatment of SARS-CoV-2 infection in the oropharyngeal cavity. The data suggest that supplementation of polyP might contribute to a strengthening of the human innate immunity system in compromised, thrombocytopenic COVID-19 patients.

1. Introduction

Among the coronaviruses, three of them causing severe pneumonia in humans have crossed the species barrier; the severe acute respiratory syndrome coronavirus (SARS-CoV), the Middle-East respiratory syndrome coronavirus (MERS-CoV), and the SARS-CoV-2 [1,2]. These three related strains belong to the β-coronavirus genus. Until today no widely approved therapeutics or vaccines have been developed against any of these human-infecting coronaviruses. As other coronaviruses also these strains show a pronounced cell tropism [3]. Cell culture studies revealed differences in cell tropism between SARS-CoV-2 and SARS-CoV [4]. The cell entry of coronaviruses is mediated by the viral spike (S) protein that binds to the cellular receptor, the angiotensin-converting enzyme 2 (ACE2) which is found at the outer cell membranes in lungs, arteries, heart, kidney, and intestines [5,6]. Prior to binding, the S-protein undergoes activation/priming by the cellular proteases furin which mediates cell attachment and TMPRSS2 which triggers membrane fusion [7,8]. The SARS-CoV S – ACE2 interaction determines the SARS-CoV transmissibility [9]. The receptor binding domain (RBD) at SARS-CoV-2 S for ACE2 has been narrowed down to the amino acid (aa) residues 328–550 at the SARS-CoV-2 S-protein sequence [3,10,11]. This RBD sequence has a theoretical isoelectric point of 8.9 which is due to a surplus of basic aa (9 Arg + 12 Lys + 1 His; 22) over acidic aa (9 Asp + 6 Glu; 15). Consequently, the RBD allows heparins, presenting pure polyanionic surfaces, to interact with S-protein [12]. Additionally, a putative glycosaminoglycan (GAG) binding motif has been identified not only at the S1/S2 proteolytic cleavage site but also more outside of this area [13]. In turn, the authors conclude that a competitive interaction of heparin with the GAG-binding-like site/motifs within SARS-CoV-2 spike glycoprotein represents a new target for an advanced carbohydrate-based COVID-19 therapeutic development.

Functional studies revealed that inorganic polyphosphate (polyP), like heparin interacts with the coagulation factor VII-activating protease [14]. This physiological polymer, polyP (reviewed in: [15]), has recently gained interest since it elicits morphogenetic activity during tissue regeneration [16] and acts as extracellular generator of metabolic energy [17]. The highest cellular level of polyP has been identified in blood platelets (see: [18]). Interestingly, it has been proposed that patients with SARS-CoV-2 show the clinical picture of thrombocytopenia

* Corresponding authors.
E-mail addresses: wang013@uni-mainz.de (X. Wang), wmueller@uni-mainz.de (W.E.G. Müller).

https://doi.org/10.1016/j.bcp.2020.114215
Received 8 July 2020; Received in revised form 13 August 2020; Accepted 3 September 2020
Available online 06 September 2020
0006-2952/

due to an increased platelet consumption paralleled with an intensified platelet destruction over the course of COVID-19 pneumonia [19]. A major pool of platelets is formed from haematopoietic progenitors/megakaryocytes during passage through the lung [20]. The deficiency in platelet counts results in a decrease not only of cytokines/chemokines but also of polyP, which is primarily stored in the platelets [15]. Even though polyP exists and is synthesized in every cell, the platelets are the main producer of the polymer. Within the cell polyP is synthesized adjacent to the mitochondria in the acidocalcisomes [21]. From this organelle the polymer is translocated to the cell membrane from where it is released, after platelet activation, into the extracellular space in two factions. First, polyP is secreted from the platelet acidocalcisomes as dense granules and retained on the outer cell surface as spherical nanoparticles (NP) which are complexed with divalent metal ions. The NP have of a size of ≈150 nm [18,22]. Second, polyP is transported into the extracellular space as non-complexed polyP in a molecularly dissolved form. Importantly, the NP associated polyP fraction contains 200 or more phosphate units, while the secreted form of the polymer is only a 60–100 residues long. The membrane-associated polyP NP, containing long-size polyP, potently activate factor XII, and in contrast, the soluble short-size polyP does not cause the activation [22]. The salt formation of polyP with Ca^{2+} or Mg^{2+} in the NP is a reversible process, since it involves a Ca^{2+} coordination to phosphate monomeric units within the polymer chain [23].

Severe coagulation abnormalities which are associated with low platelet counts [24] often occur in COVID-19 patients. Therefore, substitution of the patients with polyP appears to be indicated. Since the platelet count does not decrease to critical levels in some COVID-19 patients, we hypothesize that in those asymptomatic patients polyP has a protective function. In this study we present data indicating that polyP is interacting with the RBD at the S1 subunit of S-protein via its basic amino acids and is thereby preventing its binding to ACE2. This effect was proven with an assay system where the ACE2 protein was attached to the well plate and the labeled S-protein of SARS-CoV-2 was used as a detector molecule. Surprisingly we found that not only the Na^+ salt of the short-chain $polyP_{40}$ but also the very short polyP trimer (Na-$polyP_3$) acts strongly inhibitory down to a concentration of 1 μg/mL. This level is close to the level of polyP found in blood where this polymer is released from fully activated platelets [15,25].

PolyP, if present in the soluble, non-complexed form, is prone to enzymatic hydrolysis by the alkaline phosphatase (ALP) [26]. Therefore, short-chain polyP was fabricated into NP by complexation with divalent metal ions (Ca^{2+} or Mg^{2+}) [27]. Those particles are more resistant to ALP hydrolysis [28]. In the present study the polymer was co-precipitated with a silane precursor to form silica/polyP-NP that allowed the preparation of a suspension of polyP into a flushing solution. Silica NP are often used for biomedical applications due to their biocompatibility, comparably low cell toxicity and scalable availability (reviewed in: [29]). Moreover, strategies have been developed to reduce or avoid potential toxicities in vivo. Here, it is shown that silica/polyP-NP do not cause any growth inhibiting effect in vitro but, like the soluble $polyP_{40}$ and $polyP_3$, strongly interfere with the binding of S-protein to ACE2 via its polyP constituent. Therefore, we propose that substitution of blood and also of oropharyngeal mucus, covering the surface epithelium of intrapulmonary airways [30], with short-chain polyP might contribute to a protection against or treatment for SARS-CoV-2.

2. Materials and methods

2.1. Materials

Sodium tripolyphosphate [3 phosphate (P_i) units; $polyP_3$] was purchased from Sigma (#238503; Taufkirchen; Germany) and Graham's salt (25 P_i units; $polyP_{25}$) from Merck (#106529; Darmstadt; Germany). Na-polyphosphate (Na-polyP) with an average chain length of 40 P_i units (Na-$polyP_{40}$) was from Chemische Fabrik Budenheim (Budenheim; Germany).

2.2. PolyP size fractionation

The different polyP samples, Na-$polyP_3$, Na-$polyP_{25}$ and Na-$polyP_{40}$, were separated by 7 M urea/16.5% polyacrylamide gel electrophoresis and then stained with *o*-toluidine blue. The standards of defined chain lengths were run in parallel [26].

2.3. Preparation of silica/polyP nanoparticles

SILICA NP: The Stöber synthesis was applied [31], which is performed as a one-pot reaction at room temperature and under alkaline conditions in ethanol:water mixtures. The method avoids potentially toxic organic solvents and surfactants. In brief, 60 mL of distilled water, 30 mL of ethanol (#9065; Roth, Karlsruhe; Germany) and 10 mL of ammonium hydroxide solution (25%; #6774; Roth) were mixed and kept at 50 °C in a closed beaker. After addition of 4 mL of TEOS (tetraethyl orthosilicate; #86578 Sigma), also at 50 °C, and stirring for 4 h (50 °C) colloidal silica NP are formed. The NPs were collected by centrifugation (5,000 xg; 10 min), the supernatant was discarded, and the pellet was washed 3-times with ethanol–water (50/50 [v/v]). Finally, the silica NP were dried for 34 h at 24 h; "silica-NP". SILICA/POLYP NP: The silica-polyP NP were similarly prepared. The water/ammonia solution (60 mL) was supplemented with 0.1 g of $polyP_3$ or $polyP_{40}$. Then ethanol (30 mL) was added. Finally, the reaction mixture was supplemented with 4 mL of TEOS then processed at 50 °C as above; silica/polyP-NP either as "silica/$polyP_3$-NP" or "silica/$polyP_{40}$-NP", respectively.

2.4. Inhibition of binding of ACE2 to S-protein

The studies were performed with the spike RBD (SARS-CoV-2):ACE2 Inhibitor Screening Assay Kit (BPS Bioscience/Tebu-bio, Offenbach; Germany). This binding assay is based upon the interaction between ACE2 (50 ng/well), bound to the bottom of the 96 well plate, with the RBD of SARS-CoV-2 S1-protein (100 ng/well), labeled with biotin. The complex SARS-CoV-2 S – ACE2 is detected with streptavidin-HRP (horseradish peroxidase) followed by addition of the HRP substrate [together with the enhanced chemiluminescence reagents], producing chemiluminescence. The inhibitor, polyP, was added to the RBD of the S1-protein and, after a preincubation period of 60 min (23 °C), exposed to the ACE2. Finally, the chemiluminescence was quantitated with a Perkin Elmer-Wallac victor 3 V multi-label microplate reader (Perkin-Elmer, Waltham, MA; USA). The values for the blank (consisting of the immuno buffer used for the removal of loosely bound components in the system as well as the buffer applied for dissolving the inhibitor) were subtracted from the readings. The values obtained for the samples with the inhibitor were referred to the positive controls (containing the buffers and the labeled S-protein) which were set 100%.

If not mentioned otherwise, the samples (polyP formulations) were prepared in 10 mM HEPES [4-(2-hydroxyethyl)piperazine-1-ethanesulfonic acid] buffer, pH 7.0. The polymer was incubated with the RBD for 1 h prior to the addition to the ACE2. After blocking/washing the samples were measured. Incubation was performed at 23 °C. In one series of experiments the S-protein was incubated with $CaCl_2$ prior to addition of polyP. After an incubation period of 1 h the other components were added.

Where indicated a 10 mM MES [4-morpholineethanesulfonic acid; #M8250; Sigma] buffer, pH 5 (with HCl), or a 10 mM Tris [2-amino-2-(hydroxymethyl)-1,3-propanediol; #TRIS-RO Roche; Sigma] buffer, pH 9 (with HCl) was used instead of the 10 mM HEPES buffer at pH 7 (with NaOH). Furthermore, in one series the assays were run with additional 100 mM NaCl in the reaction. Finally, in some experiments, the reactions were run not only at 23 °C but also at 37 °C.

The soluble polymers, $polyP_3$ or $polyP_{40}$ (both as Na^+ salts), were added directly to the binding assay. The nanoparticles, "silica/$polyP_3$-NP" and "silica/$polyP_{40}$-NP" were pre-incubated first in the 10 mM HEPES (pH 7.0) for the indicated period of time. Since polyP is readily water soluble and silica NP almost insoluble in water at neutral pH [32], the polyP content of the particles was determined by weight loss measurement. NPs were suspended in 10 mM HEPES (50 mg) and after a period of 1 h, 3 h, 12 h and 24 h the samples were taken, centrifuged (5,000 x*g*) and dried. The residual solid state material was weighted. From these values the percentual proportion of water soluble (polyP) material was calculated. The results from at least three independent measurements are given.

For the determination of the effect on binding caused by "silica/$polyP_3$-NP" or "silica/$polyP_{40}$-NP" the particles were pre-incubated in the HEPES buffer (pH 7.0) and after 12 h the particle-free supernatant was collected by centrifugation. The portion of polyP released was quantified by the weighing procedure. Then, the concentrations of polyP, released, were adjusted (0, 10, 30 μg/mL) and used for pre-incubation with the S-protein in the binding assay.

2.5. Formulation of a polyP-containing flushing solution

The silica/polyP particles were suspended into a commercially used flushing solution. The liquid phase contained in 100 mL of water: dexpanthenol (0.5%), Na-benzoate (0.2 g) and anhydrous citric acid (0.01 g) [33]; all components were from Sigma. Usually 0.5 mg/mL of particles were suspended in 30 mL. The released free polyP was determined after weighing the polyP formulation before and after the incubation (1 h) - see above. Aliquots of the free polyP were subjected to the binding assay.

2.6. RBD-polyP interaction

The model of the RBD of the SARS-CoV-2 spike is based on PDB-ID: 6M0J and was deduced from PDB-ID: 6VXX and from PDB-ID: 6VYB. The RBD of SARS-CoV-2 S-protein was defined as described [3]. The delimitation of the RBD, on the aa level, has been published [10]. The model for polyP with chain length of 24 is extracted from the PDB-ID: 5llf. All molecular graphics and amino acid analyses were performed with UCSF Chimera version 1.14.

2.7. Cell culture

Human umbilical vein endothelial cells (HUVEC) were obtained from Lonza (Basel; Switzerland) and cultivated in endothelial growth medium (BulletKit-basal medium, together with SingleQuots kit) as described by the manufacturing company [34]. Cells before passage 10 were used.

2.8. Cell proliferation/cell viability XTT assay

The proliferation/viability of HUVEC was determined with the XTT Kit II ([2,3-bis-(2-methoxy-4-nitro-5-sulfophenyl)–2H-tetrazolium-5-carboxanilide]; #11465015001 Roche/Sigma) as described in the "Instructions from the Manufacturer" [35]. After an incubation period of 24 h the absorbance at 450 nm was determined and subtracted by the background values (500 nm). The values were correlated to those measured for the controls without particles and are given in percent.

2.9. Fourier transform infrared spectroscopy

The FTIR analyses were performed with an attenuated total reflectance-FTIR spectroscope/Varian IR spectrometer (Agilent, Santa Clara; CA). Ground particles were analyzed.

2.10. Energy dispersive X-ray spectroscopy

The EDX (energy dispersive X-ray spectroscopy) analyses were performed with an EDAX Genesis EDX System which was online with the scanning electron microscope (Nova 600 Nanolab; FEI Company, Hillsboro; OR). The detector operated at 10 kV and a collection time of 30–45 s. To achieve a (semi)-quantitative result the system was calibrated [36]. The results had a standard error of ~10%.

2.11. Microscopic analyses

Electron microscopy was performed with a scanning electron microscope (SEM), a HITACHI SU8000 electron microscope (Hitachi, Krefeld; Germany). Transmission electron microscopy (TEM) was performed with a Tecnai 12 (FEI, Eindhoven, The Netherlands) at an accelerating voltage of 120 kV.

2.12. Statistical analysis

The values reported are the average ± standard deviations (σ). Student *t* test was applied to perform comparisons between two groups. Usually the average values and σ originated from at least three to six independent experiments. Due to the high sensitivity of the chemiluminescence assay, less frequently also results were included that came from different assays which produced different levels for their included positive controls. Values of $p < 0.05$ were considered statistically significant (*). IC_{50} estimation was performed using the regression techniques [37]. The calculations were performed with the GraphPad Prism 7.0 software (GraphPad Software, La Jolla; CA).

3. Results

3.1. The interaction of RBD with polyP

The RBD of SARS-CoV-2 comprises a solvent-accessible surface area that is exposed to the aqueous surrounding environment of the protein [12]. The sites that are suspected to command ligand-receptor mediated conformational changes [38] are found at the surface of the RBD as a continuous stretch of the basic aa Arg and Lys. Arg as the most basic of all amino acids is under physiological conditions always protonated and has the propensity to form intramolecular salt bridges [39]. To elucidate if the RBD with its solvent-accessible surface area comprise a space-filling region for polyP a molecular modeling approach was performed.

After retrieval of the RBD of SARS-CoV-2 S-protein and of the model for polyP with a chain length of 24 phosphate units, a space filling model was built (Fig. 1). At the lateral side of the RBD it is evidenced that ten out of 18 aa (total aa at the RBD) that are exposed are the basic aa Arg, Lys and His (Fig. 1). Interestingly, six of those basic aa are spatially connected, allowing the docking of a polyP chain with a chain length of 15 P_i units. None of those aa is directly adjacent to conserved N-linked glycosylation sequons [3]. As deduced from this assessment, an association of polyP with a chain length of ~15 P_i units is possible via electrostatic interactions.

3.2. PolyP fractions used

For the studies here the commercially available polyP samples have been used; Na-$polyP_3$, the Graham's salt (~25 P_i) and Na-polyP (~40 P_i); they are all present in the water soluble Na^+ form. The size-separation analysis shows that the $polyP_3$ sample has a quite narrow size distribution range (2 to 5 P_i units), while $polyP_{25}$ (4 to 40 P_i) and $polyP_{40}$ (8 to 80 P_i) show a broader distribution (Fig. 2**a**). Basically this distribution is not disadvantageous since also in the circulating fluid, in the human body, a distinct dispersion cannot be expected, since the polymer is readily accessible to the hydrolyzing enzyme ALP [40]. For

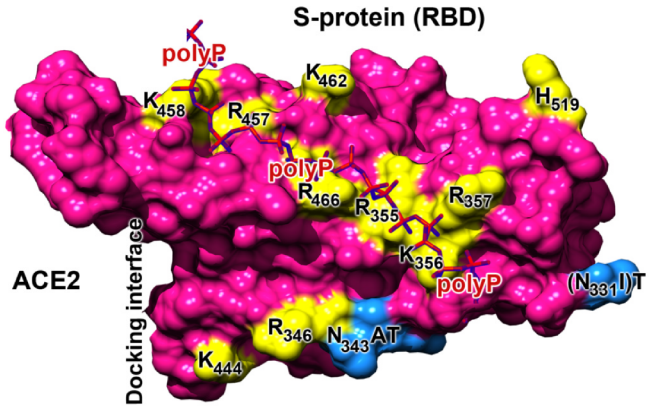

Fig. 1. Predicted interaction of $polyP_{40}$ with the SARS-CoV-2 S1 RBD. PolyP was superposed with the RBD. The non-polar and the acidic amino acids (aa) are in pink, the basic aa in yellow, while the aa with the putative N-glycosylation sites are in blue. Those aa which are proposed to bind to the polymer (polyP) are marked. In this surface model the docking interface of the S-protein with its RBD to the ACE2 is to the left. (For interpretation of the references to colour in this figure legend, the reader is referred to the web version of this article.)

the functional studies described here $polyP_3$ and $polyP_{40}$ samples were used.

3.3. Silica/polyP-NP

To stabilize the soluble polyP toward extensive attack by ALP, the water soluble Na^+ salt of the polymer was entrapped by co-fabrication with silica. The "silica-NP" were prepared following the Stöber synthesis by addition of TEOS to ammonium hydroxide in ethanol:water mixtures. The resulting particles had a diameter of 210 ± 40 nm (n = 6 determinations), as visualized by TEM (Fig. 2b (A)). Similar dimensions were also measured by SEM with ~166 ± 36 nm (Fig. 2b (C)). After co-addition of polyP to silica, here the images for the $polyP_{40}$ fabricated nanoparticles are shown ("silica/$polyP_{40}$-NP"), it becomes visible by TEM that the particles are decorated with a fluffy layer of polyP chains that protrude from the compact silica/polyP core (Fig. 2b (B)). If those particles are analyzed by SEM compact core particles are seen that are garnished with small blobs (Fig. 2b (D)).

3.4. FTIR spectroscopy analysis of the silica-NP and silica/$polyP_{40}$-NP

The spectra of both the "silica-NP" and the "silica/polyP-NP" show the characteristic symmetric and asymmetric stretching vibrational modes for Si-O-Si at ν_s 1048 and ν_{as} 791 cm^{-1}, respectively (Fig. 2c). The absorption band at 956 cm^{-1} is assigned to the asymmetric bending and stretching vibration modes of the surface silanol groups (Si-OH) [41,42]. The broad band from 3100 to 3600 cm^{-1} corresponds to the OH stretching modes of Si-OH groups and H_2O and the weak band 1640 cm^{-1} is due to the OH bending vibration in water. This finding reflects the silica scaffold in the NP that is synthesized after hydrolysis and condensation of TEOS. These signals are also seen in the two "silica/polyP-NP" formulations, "silica/$polyP_3$-NP" and "silica/$polyP_{40}$-NP". The signature for polyP is present at the vibrational mode for P-O-P at a ν of 900 cm^{-1} [28].

3.5. Element distribution in the particles

The EDX patterns obtained from "silica-NP", "silica/$polyP_3$-NP" and "silica/$polyP_{40}$-NP" are given in Fig. 2d. In the spectrum of "silica-NP" the signals for O and Si appear, while the peaks for P and Na are absent (Fig. 2d (A)). In contrast, the patterns for "silica/$polyP_3$-NP" and "silica/$polyP_{40}$-NP" show the distinct peaks for both P and Na (Fig. 2d (B and C)). The Wt% for phosphate in the fractions was determined with 13.0 ("silica/$polyP_3$-NP" [P content: 5.1 ± 0.7 wt%]) and 24.4 wt% ("silica/$polyP_{40}$-NP" [P: 9.6 ± 0.9 wt%]), respectively.

3.6. PolyP release kinetics

The release of polyP from the silica/polyP-NP was measured on the basis of the time-dependent weight loss if suspended in aqueous 10 mM HEPES (pH 7.0). In Fig. 3**a** the data are graphically illustrated. For both particles "silica/$polyP_3$-NP" and "silica/$polyP_{40}$-NP" the release occurs in a biphasic manner, with rapid liberation during the first 3 h, followed by a slower release during the following 21 h. Interestingly, the values obtained agree with the P_i content measured by EDX with 13.0 wt% (release: 12.5 ± 1.7 wt%) for "silica/$polyP_3$-NP" and with 24.4 wt% (release: 21.4 ± 1.8) for the "silica/$polyP_{40}$-NP" sample. The rapid burst of polyP release from the particles during the first 3 h is attributed to the polyP molecules that are protruding out of the surfaces of the particles, while the subsequent slower release reflects the leaching from the silica core of the hybrid particles.

3.7. Reduced toxicity of silica/$polyP_{40}$-NP versus silica-NP

The growth/viability of the HUVEC cells, in dependence on exposure to NP (either "silica-NP" or "silica/$polyP_{40}$-NP"), was determined with the XTT assay system. After incubation, the mean viability of cells exposed to "silica-NP" decreases concentration-dependently. Already after 24 h the number of cells in the 10 μg/mL assays decrease by 32%, and at 30 μg/mL by 52% (Fig. 3b). In contrast, if the NP were fabricated with $polyP_{40}$, "silica/$polyP_{40}$-NP", no toxicity of the NP is seen. Even more, the viability increases significantly ($p < 0.05$) at the concentration of 10 μg/mL, and the formulation "silica/$polyP_{40}$-NP" remained non-toxic at the higher concentrations tested. In parallel, the effect of "silica/$polyP_3$-NP" on HUVEC has likewise been tested. Again these particles, in the concentration range up to 100 μg/mL, had no toxic effect on the cells during the 24 h incubation period (data not shown).

3.8. Inhibition of binding of S-protein to ACE2 by soluble polyP

The two soluble polyP size-factions, $polyP_3$ and $polyP_{40}$, were tested in the binding assay for their inhibitory potential on the interaction of S-protein and ACE2. The two polyP samples used here, $polyP_3$ and $polyP_{40}$, inhibit binding of the RBD to the ACE2 down to the concentration of 1 μg/mL (Fig. 3c). This inhibition is significant with a $p < 0.005$. Already at 1 μg/mL of $polyP_{40}$ the reduction of binding is 27%. At concentrations higher than 10 μg/mL, the binding inhibition increases to 71%. Stronger than the effect of $polyP_{40}$ is the inhibitory activity caused by Na-$polyP_3$. With this shorter polymer and at a concentration of 10 μg/mL, a decrease of binding to ~40% is measured, if compared to control. The IC_{50} values could be assessed approximately with 34 ± 15 μg/mL for $polyP_{40}$ and with 7.8 ± 12 μg/mL for Na-$polyP_3$.

3.9. Strength of interaction between RBD (ACE2) and polyP in dependence on pH, ionic strength and temperature

In a comparative series of experiments the effects of 30 μg/mL of $polyP_{40}$ on the interaction between RBD and ACE2 under different pH conditions, by changing the ionic strength in the assay reaction and finally at different temperatures were determined (Fig. 4).

The pH in the reaction assay was adjusted to pH 5 with 10 mM MES, to pH 7 with 10 mM HEPES, or to pH 9 with 10 mM Tris. After incubation of the RBD with 30 μg/mL $polyP_{40}$ and the subsequent incubation with ACE2 a ~40% inhibition is measured for all pH conditions (Fig. 4a). The differences between the three test groups are not statistically significant.

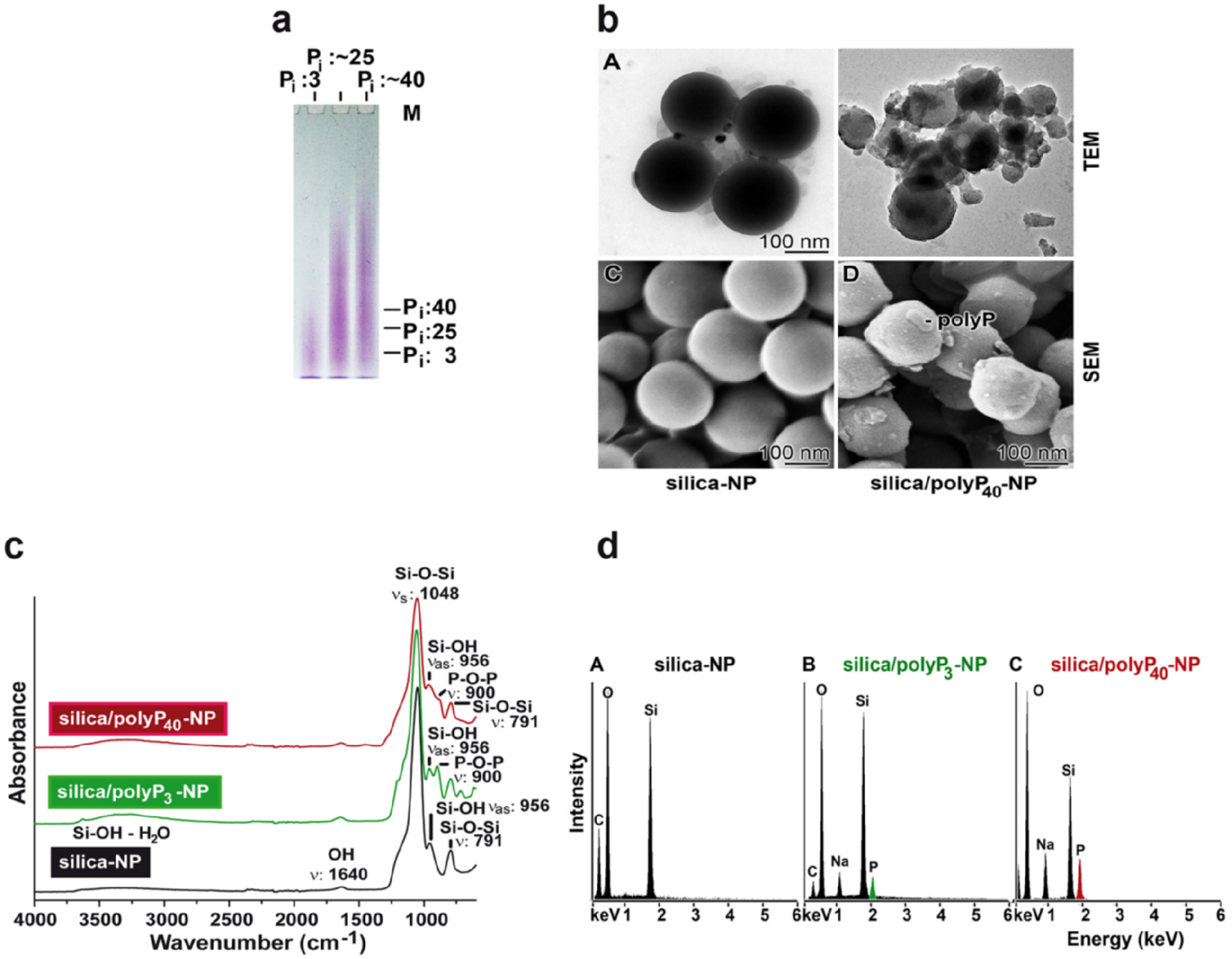

Fig. 2. Characterization of polyP. a Fractionation of polyP samples by 7 M urea/16.5% polyacrylamide gel electrophoresis. The samples Na-polyP$_3$ (3 P$_i$ units), Graham's salt (~25 P$_i$) and Na-polyP (~40 P$_i$) were separated. Purified polyP size markers were run in parallel. b Morphology of both "silica-NP" and "silica/polyP$_{40}$-NP". Analysis of (A and B) "silica-NP" and "silica/polyP$_{40}$-NP" by TEM, as well as of (C and D) "silica-NP" and "silica/polyP$_{40}$-NP" by SEM. The decorations of the solid silica/polyP core with free polyP chains are marked (polyP). c The FTIR spectral characteristics of "silica-NP" as well as of the polyP containing "silica/polyP$_3$-NP" and "silica/polyP$_{40}$-NP" samples. Typical signal peaks for the silica matrix (two Si-O-Si; Si-OH) and for the polyP additives (P-O-P) are marked. d The EDX pattern of the formulations "silica-NP", "silica/polyP$_3$-NP" and "silica/polyP$_{40}$-NP". In the hybrid particles also the P signals are visible.

In parallel, the reaction was performed in the absence and in the presence of 100 mM NaCl. Again, the strength of inhibition, caused by polyP, between the two groups was statistically not different (Fig. 4b).

In the last test series the reaction was run at 23 °C (used for the routine studies) and at 37 °C. The degree of inhibition was significantly lower at the higher incubation temperature (Fig. 4c).

3.10. Inhibition of binding of S-protein to ACE2 by particle-associated polyP

Next the polyP released from "silica/polyP$_3$-NP" and "silica/polyP$_{40}$-NP" (see Fig. 3a) was determined for its inhibitory activity As outlined, from those NP polyP is released, especially fast during the first 12 h. It was found that 10 μg/mL of polyP (released from "silica/polyP$_3$-NP") reduced the binding of SARS-CoV S to ACE2 by 38%, while the same amount from "silica/polyP$_{40}$-NP" caused a decrease to approximately the same extent (Fig. 3d).

3.11. Inhibitory activity of free polyP in flushing solution

The polymers Na-polyP$_3$ and Na-polyP$_{40}$ were tested in the free, Na^+ salt form in a mouth flushing solution for their effects on the binding S-protein – ACE2 (Fig. 3e). The two polyP samples at concentrations of 10 and 30 μg/mL significantly inhibited the binding of the two components. The reduction of binding by the preparations is ~40%.

3.12. Reduction of polyP effect on binding by Ca^{2+}

In a separate series of experiments the S-protein was incubated with 0, 2 or 5 mM Ca^{2+} (addition in form of $CaCl_2$). After 1 h the assay was processed with the other components in the absence or presence of polyP. In the presence of 2 mM Ca^{2+} the inhibitory activity of 3 μg/mL of polyP$_{40}$ was already significantly reduced (to 82 ± 7%); addition of 5 mM Ca^{2+} caused an almost complete suppression of inhibition (to 89 ± 8%), in comparison to the inhibitory activity seen for the soluble, free Na-polyP in the absence of Ca^{2+}.

4. Discussion

The RBD [10] of the SARS-CoV-2 S-protein is a sequence that is exclusively found in SARS-CoV-2 with the high expect value ($2e^{-166}$; PDB: 6M0J_E). Already much lower is the e-value for other spike

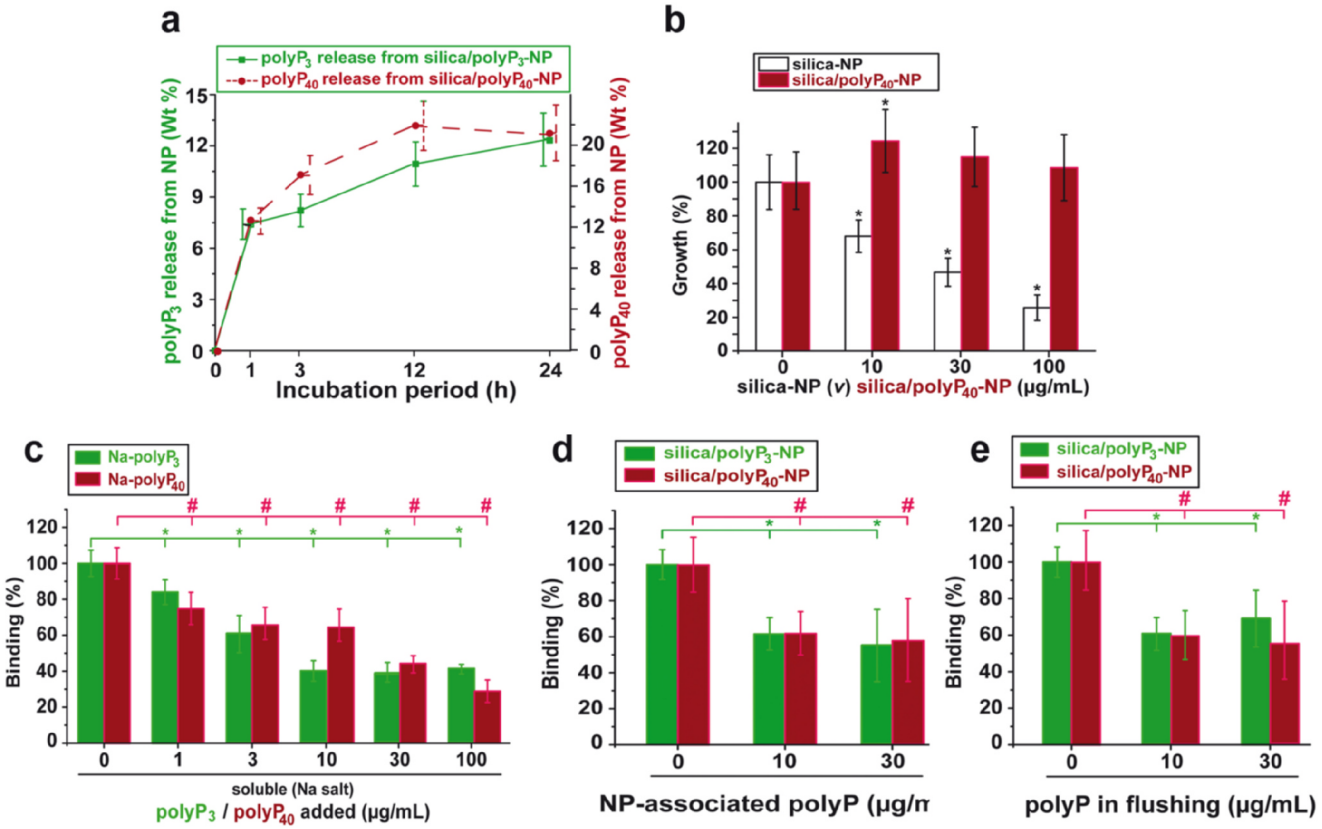

Fig. 3. *In vitro* studies. a The in vitro polyP release from the "silica/polyP$_3$-NP" as well as from the "silica/polyP$_{40}$-NP" particles. The kinetics show a biphasic profile; fast release during the first 3 h, and slow release thereafter. b The viability of HUVEC cells in the presence of either "silica-NP" or "silica/polyP$_{40}$-NP". The cells were incubated for 24 h and then subjected to the XTT assay. Ten parallel experiments were performed and the mean values (± SD) are shown. Significant correlations to the controls (no addition of NP), either decrease of growth ("silica-NP") or enhanced growth ("silica/polyP$_{40}$-NP") are marked (*, $p < 0.05$). c Impairment of SARS-CoV-2 S – ACE2 binding by the two Na-polyP fractions. The binding between the RBD of SARS-CoV-2 S and ACE2 was measured in the presence of different concentrations of polyP$_3$ or polyP$_{40}$ (Na-salts); the binding values between the two components are given in percent. The positive controls without polyP are set to 100%. Data came from 6 parallel experiments; means ± SEM are given (*, $p < 0.05$). d Effect of polyP, released from the silica/polyP NP, on the binding of S-protein to ACE2. The indicated amounts of polyP$_3$ or polyP$_{40}$ (polyP released) were pre-incubated with the RBD of S-protein and then added to the ACE2 composed binding assay. Means ± SEM (*, $p < 0.05$). e Inhibition of the SARS-CoV-2 S – ACE2 binding by free Na-polyP$_3$ or polyP$_{40}$, release from the NP in the flushing solution. The polyP samples were dissolved in the solution for 1 h and then added to the binding system. Means ± SEM (*, $p < 0.05$).

surface glycoproteins, like for the human coronavirus OC43 (PDB: 6NZK_A) with $2e^{-09}$. Interestingly enough, an amino acid sequence similarity search of the published RBD revealed that even between the most distantly related sequence from the RBD of SARS-CoV-2, the reference sequence used in the present study the chain E, spike glycoprotein (from the SARS-CoV-2; accession number 6XDG_E, with an expect value $4e^{-160}$) and the more distantly related spike glycoprotein (accession: QKV25357; with an $2e^{-149}$), none of the Arg residues have

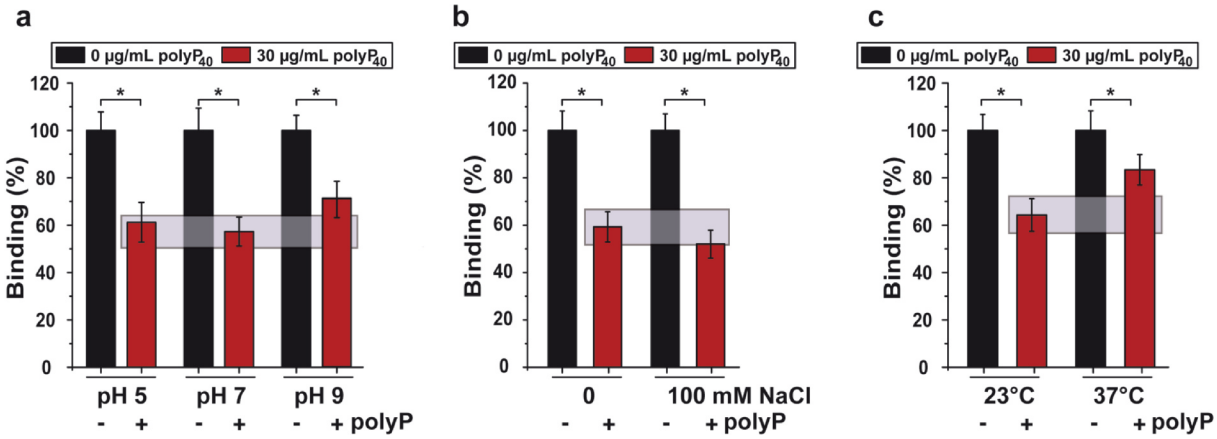

Fig. 4. Strength of inhibition in dependence on different pH, ionic strength and incubation temperature. The standard incubation assay was used, except of a different pH conditions in the assays (pH 5 [MES buffer]; pH 7 [HEPES buffer]; pH 9 [Tris buffer]) or of b additional NaCl. c In the last series, the experiments were performed at 23 °C and at 37 °C. Means ± SEM (*, $p < 0.05$). The transparent horizontal bars indicate the strength of inhibition (SEM limits) under standard condition conditions, at pH 7, without NaCl and at 23 °C.

been changed or deleted. Therefore, this finding might suggest that mutations, occurring in the spike glycoprotein, do not extend to the RBD.

No significant similarity is found for the viral RBD sequence to other metazoan sequences. The RBD does not show any defined and listed domain, like in CDART [43], which could hint to a putative function as a ligand or a receptor. The theoretical isoelectric point (pI) of RBD is 8.9, reflecting the abundance of basic aa over acidic aa. Instructive are the pIs of the basic aa Arg (pI of 10.8), Lys (9.5) and His (7.5) indicating that below these values these aa are positively charged. In turn, at physiological pH values the basic aa moieties react cationically. Interestingly, the airway surface liquid is normally acidic relative to the blood pH of around ~6.6 [44]. This value drops significantly during pneumonia to pH 6.48 [45]. This would imply that during an inflammation of the lungs the basic aa of the RBD of the S-protein (at the Arg sites) are prone to a putative binding for (poly)anions. Two flexible polyanionic and adaptive polymers exist physiologically in the blood; they are heparin (~1 μg/mL [46]) and polyP (~0.3 μg/mL [15]). Heparin is synthesized in mast cells, while the related glycosaminoglycan heparan sulfate is basically produced in all cells of the human body [47]; polyP is likewise synthesized in all human cells but primarily delivered to the blood by the platelets [15]. It has been reported that during coronavirus infection immune cells, including mast cells from the submucosa of the respiratory tract, attack the virus [48] suggesting that from some immune cells, mast cells and/or blood platelets, polyanions might be released that could contribute to a better prognosis of severe COVID-19 patients [49].

The strength of interaction between the RBD and the ACE2 receptor has not been studied until now. One reason might be the lack of sufficient amounts of recombinant protein for e.g. surface plasmon resonance analyses [50]. Therefore, the assessment of the binding strength between these two components to each other and to the inhibitor of this interaction, to polyP, had to be performed in another way. We propose in the presented study an electrostatic interaction between polyP and Arg amino acids, existing at the surface of the RBD. The strength of those interactions has been attributed to be strong and “covalent-like” [51]. The Arg moieties can also form salt bridges if these amino acids are flanked by acidic Glu or Asp amino acids [52]. In the RBD adjacent to Arg_{457} (Fig. 1), one Glu_{465} and one Asp_{467} are arranged at the surface of the molecule [3]. Under those amino acid arrangements the binding of the Arg residues via their guanidinium groups to phosphate is favored compared to an interaction with the adjacent carboxyl groups both in Asp and in Glu [53]. In our approach, we determined the binding strength of polyP to the RBD and to the ACE2 by varying the pH and the ionic strength in the binding assay, as well as the incubation temperature within the physiological range. It is found that within the pH range 5 to 7, and in the presence of 0 or 100 mM NaCl, the polyP caused inhibition of the RBD – ACE2 interaction is not affected. Only at an elevated temperature (37 °C instead of 23 °C) the inhibition was reduced, but was still present. These results indicate that once the noncovalent bond is established between polyP and the Arg residues, a thermodynamically highly favorable and stabile conformation has been reached. Such a strong Arg-phosphate electrostatic interaction has been described for interactions between basic epitopes containing adjacent Arg residues and acidic epitopes, at a phosphorylated Ser, during receptor heteromerizations [51].

PolyP causes a reduction of the RBD binding to ACE2 by about 70%. This incomplete inhibition might be due to an only partial/cryptic exposure of the Arg residues on the RBD surface. Therefore, Arg residues on the RBD surface had been modified with 1,2-cyclohexanedione in a Na-borate buffer (pH 9) [54]. After this modification an increased inhibition of the binding between the RBD and ACE2 was measured (W.E.G. Müller; to be published). In addition, the limited inhibitory effect of polyP might be attributable to only a partial, restricted effect of polyP on the RBD – ACE2 complex. As outlined in the “Introduction” the attachment and entry of the virus is a complex process and involves a series of sequential enzymatic cleavages and binding associations [7–9].

Increasing evidence has been reported that the platelet count drops during corona pneumonia [19]. The task of the present study was to elucidate if the physiological polymer polyP can bind to the surface of the SARS-CoV-2 S-protein via electrostatic linkages. The geometry and the spacing between two aa within the peptide perfectly fit with the length of 2.0 to 2.5 Å [55]. These distances match noticeably well with the length in the polyP chain between two phosphate anhydride linkages of 2.7 Å [17]. Building the surface model of RBD it becomes overt that six aa, Arg and Lys, exposed on the lateral surface, are almost continuously forming a path (Fig. 1), allowing six to eight P_i units within the polyP chain to bind to the S-protein in an end-to-end orientation.

We describe for the first time that $polyP_{40}$ causes an inhibitory effect on the interaction of the viral S-protein with the cellular receptor ACE2. The data suggest that polyP binds to the patches of basic aa on the surface of RBD and prevents binding to ACE2. The potential of polyP to form electrostatic linkages both to biomolecules and divalent metal ions is well proven [56]. An example is the strong interaction of the anionic polyP with basic aa in proteins [57]. Subsequently, after interaction of polyP with the S-protein, a conformational change of the S-protein is likely to proceed. Such a transformation within the RBD is well proven [12,58]. In the main series of experiments polyP samples with chain lengths of ~40 P_i units and with 3 P_i have been selected. The $polyP_{40}$ molecules surely will show an overhang of about 15 P_i units over the lateral surface of the RBD and have the steric potential to dock additionally onto the opposing ACE2 molecule. If so the polyP chain can bend and turn around its anhydride linkages [17], allowing the same polyP molecule to bind not only to the RBD but, after forming a hairpin turn, also to the approaching ACE2 receptor. Exactly at this interface five basic aa are present at the ACE2 that could abolish, after binding of polyP, the binding propensity of the RBD for the ACE2. Focusing on the inhibitory activity of $polyP_3$ a series of potential sites on the surface of both RBD and ACE2 exist. These basic aa are highlighted in the S-protein in Fig. 1 in yellow. On a stoichiometric base, the binding ratio between Na-$polyP_{40}$ (MW: 4240 g/mol) at 1 μg/mL and the RBD (molecular mass of 24.5 kDa) is 2.9:1, while the ratio Na-$polyP_3$ (MW: 318 g/mol) to RBD is 40:1, suggesting a cooperative binding of $polyP_{40}$.

PolyP in the blood is assumed not to be long-living since the medium is rich in the hydrolyzing enzyme ALP. Therefore, the soluble polyP polymer was encapsulated into a silica core. Those particles with a diameter of ~150 to 200 nm show protruding polyP chains that are more loosely integrated into the core particles. EDX as well as FTIR studies proved that the particles are composed both of polyP and of silica. PolyP was encapsulated into the silica particles in the absence of any divalent metal ion like Mg^{2+} or Ca^{2+}. This technique allowed an encapsulation of the polymer in a non-chelated, free polyP state. By this, the polymer retains its complexation activity and does only slightly impair the hydrolytic activity towards the ALP enzyme [26]; in the presence of the enzyme only a ~20% slower release was measured (unpublished). This property is considered as important, since the binding of polyP to S-protein most likely occurs via electrostatic interactions. A direct proof was obtained by showing that after addition of $CaCl_2$ to the binding system, Ca^{2+} blocks the binding propensity of polyP for the positively charged, basic side chains of Lys, Arg or His at the RBD. The binding affinity of phosphate residues to Ca^{2+} is high and increases progressively with an increase of the chain length [59]. The binding propensity of Zn^{2+} is similarly high compared to the one to Ca^{2+}; consequently it can be deduced that chelation of Zn^{2+} might reduce the enzymatic activity of ACE2 [60]. The role of polyP on the binding partner ACE2 needs to be studied.

Silica NP can cause cell toxicity in vitro, which is dependent on the size and dose of the NP and also on the cell type studied [61]. In the system used here an approximately 50% inhibition is measured at concentrations around 30 μg/mL for HUVEC cells. Supplementation of

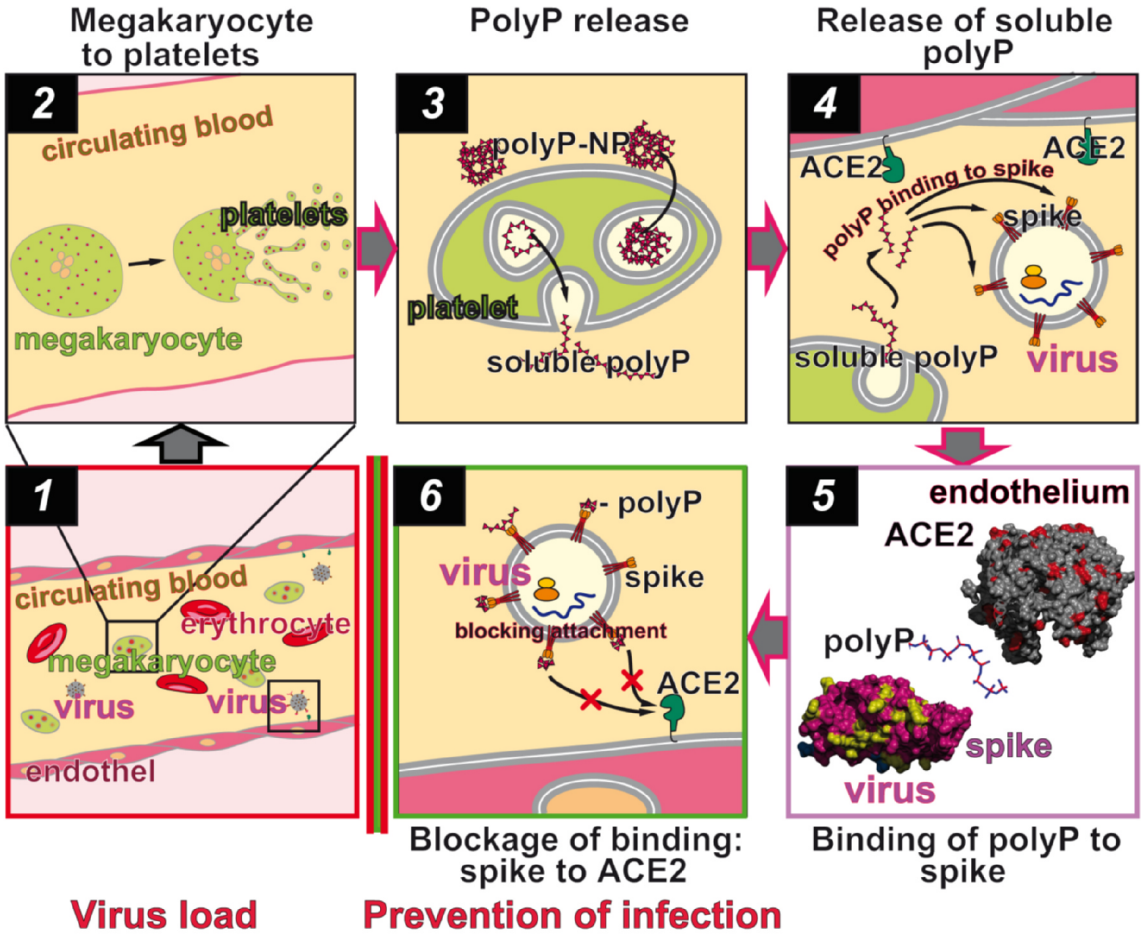

Fig. 5. The innate immunity concept with polyP as the central point. (Step-1) Virus load in the blood circulation system. (Step-2) Development of blood platelets from the megakaryocytes. (Step-3) Release of two fractions of polyP from the platelets, the free soluble polyP chains (short-chain) and the particle-bound polyP (long-chain). (Step-4) The short-chain polyP molecules are floating within the blood and bind there to the S-protein of the virions. (Step-5) Binding of the polyP chains to the virus spike protein and the interface between S-protein and ACE2. (Step-6) Prevention of attachment of the virions to the host endothelial cell membranes.

those particles with $polyP_{40}$ abolished cell growth inhibition. This effect is attributed to the morphogenetic activity elicited by polyP [16,17].

In conclusion, in the present study we report on the role of polyP during the binding of the two crucial partners of the initial phase of corona virus infection, SARS-CoV-2 S and ACE2. This interaction has been narrowed down to a strong interaction of the polyanionic physiological polymer with the stretch of basic aa localized on the surface of the RBD of S-protein (Fig. 1). These data suggest that polyP plays a crucial role during the initial phase of infection (Fig. 5). Evidence suggests that platelets accumulate at the site of infection (Fig. 5-Step 1) [62]. There, the platelets become activated (Fig. 5-Step 2) and engulf virions, with the human influenza virions as an example. In addition, the platelets expose/release granules involved in Toll-like receptor (TLR) signaling events [63]. Subsequently, activated platelets release polyP into the blood (Fig. 5-Step 3) and allow the free floating inorganic polyP to bind to the spike S-protein (Fig. 5-Step 4). The binding of polyP to the RBD of S-protein has been demonstrated in this study (Fig. 5-Step 5). Finally, S-protein is unable to bind to ACE2 (Fig. 5-Step 6) with the consequence of a blockade of infection.

Since this polyP-mediated control of virus propagation is a physiological one and most likely compromised during SARS-CoV-2 infection, polyP can be considered as a further major arm of the body's strategy to fight against SARS-CoV-2, in addition to the TLR-mediated response and the activation of the complement system.

Acknowledgements

We would like to acknowledge and thank Mr. Gunnar Glasser (Department of Physical Chemistry of Polymers; Max Planck Institute for Polymer Research; Mainz – Germany) for his expert electron microscopy contributions. W.E.G. M. is the holder of an ERC Advanced Investigator Grant (no. 268476). In addition, W.E.G. M. has obtained three ERC-PoC grants (Si-Bone, no. 324564; MorphoVES-PoC, no. 662486; and ArthroDUR, no. 767234).

Conflict of interest

The authors declare no conflict of interest.

Author contributions

W.E.G.M., I.L., H.C.S. and X.H.W. conceived and supervised the entire project. M.N., E.T. and S.F.W. prepared the materials and carried out the studies. All authors carried out the analyses, discussion and revisions.

References

[1] C. Drosten, S. Günther, W. Preiser, S. van der Werf, H.R. Brodt, S. Becker, H. Rabenau, M. Panning, L. Kolesnikova, R.A. Fouchier, A. Berger, A.M. Burguière, J. Cinatl, M. Eickmann, N. Escriou, K. Grywna, S. Kramme, J.C. Manuguerra, S. Müller, V. Rickerts, M. Stürmer, S. Vieth, H.D. Klenk, A.D. Osterhaus, H. Schmitz, H.W. Doerr, Identification of a novel coronavirus in patients with severe acute

respiratory syndrome, N. Engl. J. Med. 348 (2003) 1967–1976.
[2] C. Huang, Y. Wang, X. Li, L. Ren, J. Zhao, Y. Hu, L. Zhang, G. Fan, J. Xu, X. Gu, Z. Cheng, T. Yu, J. Xia, Y. Wei, W. Wu, X. Xie, W. Yin, H. Li, M. Liu, Y. Xiao, H. Gao, L. Guo, J. Xie, G. Wang, R. Jiang, Z. Gao, Q. Jin, J. Wang, B. Cao, Clinical, features, of, patients, infected, with,, novel coronavirus in Wuhan, China, Lancet 395 (2020) (2019) 497–506.
[3] A.C. Walls, Y.J. Park, M.A. Tortorici, A. Wall, A.T. McGuire, D. Veesler, Structure, function, and antigenicity of the SARS-CoV-2 spike glycoprotein, Cell 181 (2020) 281–292.
[4] D. Bojkova, J.E. McGreig, K.M. McLaughlin, S.G. Masterson, M. Widera, V. Krähling, S. Ciesek, M.N. Wass, M. Michaelis, J. Cinatl, SARS-CoV-2 and SARS-CoV differ in their cell tropism and drug sensitivity profiles, bioRxiv 2020, doi: https://doi.org/10.1101/2020.04.03.024257.
[5] W. Li, M.J. Moore, N. Vasilieva, J. Sui, S.K. Wong, M.A. Berne, M. Somasundaran, J.L. Sullivan, K. Luzuriaga, T.C. Greenough, H. Choe, M. Farzan, Angiotensin-converting enzyme 2 is a functional receptor for the SARS coronavirus, Nature 426 (2003) 450–454.
[6] M. Hoffmann, H. Kleine-Weber, S. Schröder, N. Krüger, T. Herrler, S. Erichsen, T.S. Schiergens, G. Herrler, N.H. Wu, A. Nitsche, M.A. Müller, C. Drosten, S. Pöhlmann, SARS-CoV-2 cell entry depends on ACE2 and TMPRSS2 and is blocked by a clinically proven protease inhibitor, Cell 181 (2020) 271–280.
[7] B. Coutard, C. Valle, X. de Lamballerie, B. Canard, N.G. Seidah, E. Decroly, The spike glycoprotein of the new coronavirus 2019-nCoV contains a furin-like cleavage site absent in CoV of the same clade, Antiviral Res. 176 (2020) 104742.
[8] I. Glowacka, S. Bertram, M.A. Müller, P. Allen, E. Soilleux, S. Pfefferle, I. Steffen, T.S. Tsegaye, Y. He, K. Gnirss, D. Niemeyer, H. Schneider, C. Drosten, S. Pöhlmann, Evidence that TMPRSS2 activates the severe acute respiratory syndrome coronavirus spike protein for membrane fusion and reduces viral control by the humoral immune response, J. Virol. 85 (2011) 4122–4134.
[9] W. Li, C. Zhang, J. Sui, J.H. Kuhn, M.J. Moore, S. Luo, S.K. Wong, I.C. Huang, K. Xu, N. Vasilieva, A. Murakami, Y. He, W.A. Marasco, Y. Guan, H. Choe, M. Farzan, Receptor and viral determinants of SARS-coronavirus adaptation to human ACE2, EMBO J. 24 (2005) 1634–1643.
[10] X. Ou, Y. Liu, X. Lei, P. Li, D. Mi, L. Ren, L. Guo, R. Guo, T. Chen, J. Hu, Z. Xiang, Z. Mu, X. Chen, J. Chen, K. Hu, Q. Jin, J. Wang, Z. Qian, Characterization of spike glycoprotein of SARS-CoV-2 on virus entry and its immune cross-reactivity with SARS-CoV, Nat. Commun. 11 (2020) 1620.
[11] M. Hoffmann, H. Kleine-Weber, S. Pöhlmann, A multibasic cleavage site in the spike protein of SARS-CoV-2 is essential for infection of human lung cells, Mol. Cell 78 (2020) 779–784.
[12] C. Mycroft-West, D. Su, S. Elli, S. Guimond, G. Miller, J. Turnbull, E. Yates, M. Guerrini, D. Fernig, M. Lima, M. Skidmore, The 2019 coronavirus (SARS-CoV-2) surface protein (Spike) S1 receptor binding domain undergoes conformational change upon heparin binding, bioRxiv 2020, doi: https://doi.org/10.1101/2020.02.29.971093.
[13] S.Y. Kim, W. Jin, A. Sood, D.W. Montgomery, O.C. Grant, M.M. Fuster, L. Fu, J.S. Dordick, R.J. Woods, F. Zhang, R.J. Linhardt, Glycosaminoglycan binding motif at S1/S2 proteolytic cleavage site on spike glycoprotein may facilitate novel coronavirus (SARS-CoV-2) host cell entry, BioRxiv (2020), https://doi.org/10.1101/2020.04.14.041459.
[14] L. Muhl, S.P. Galuska, K. Oörni, L. Hernández-Ruiz, L.C. Andrei-Selmer, R. Geyer, K.T. Preissner, F.A. Ruiz, P.T. Kovanen, S.M. Kanse, High negative charge-to-size ratio in polyphosphates and heparin regulates factor VII-activating protease, FEBS J. 276 (2009) 4828–4839.
[15] J.H. Morrissey, S.H. Choi, S.A. Smith, Polyphosphate: an ancient molecule that links platelets, coagulation, and inflammation, Blood 119 (2012) 5972–5979.
[16] X.H. Wang, H.C. Schröder, W.E.G. Müller, Amorphous polyphosphate, a smart bioinspired nano-/bio-material for bone and cartilage regeneration: Towards a new paradigm in tissue engineering, J. Mat. Chem. B 6 (2018) 2385–2412.
[17] W.E.G. Müller, H.C. Schröder, X.H. Wang, Inorganic polyphosphates as storage for and generator of metabolic energy in the extracellular matrix, Chem. Rev. 119 (2019) 12337–12374.
[18] J.I. Weitz, J.C. Fredenburgh, Platelet polyphosphate: the long and the short of it, Blood 129 (2017) 1574–1575.
[19] J.B. Larsen, L. Pasalic, A.M. Hvas, Platelets in Coronavirus Disease, Semin. Thromb. Hemost. 2020 (2019), https://doi.org/10.1055/s-0040-1710006.
[20] E. Lefrançais, G. Ortiz-Muñoz, A. Caudrillier, B. Mallavia, F. Liu, D.M. Sayah, E.E. Thornton, M.B. Headley, T. David, S.R. Coughlin, M.F. Krummel, A.D. Leavitt, E. Passegué, M.R. Looney, The lung is a site of platelet biogenesis and a reservoir for haematopoietic progenitors, Nature 544 (2017) 105–109.
[21] R. Docampo, G. Huang, Acidocalcisomes of eukaryotes, Curr. Opin. Cell Biol. 41 (2016) 66–72.
[22] J.J. Verhoef, A.D. Barendrecht, K.F. Nickel, K. Dijkxhoorn, E. Kenne, L. Labberton, O.J. McCarty, R. Schiffelers, H.F. Heijnen, A.P. Hendrickx, H. Schellekens, M.H. Fens, S. de Maat, T. Renné, C. Maas, Polyphosphate nanoparticles on the platelet surface trigger contact system activation, Blood 129 (2017) 1707–1717.
[23] A.J. Donovan, J. Kalkowski, S.A. Smith, J.H. Morrissey, Y. Liu, Size-controlled synthesis of granular polyphosphate nanoparticles at physiologic salt concentrations for blood clotting, Biomacromolecules 15 (2014) 3976–3984.
[24] P. Xu, Q. Zhou, J. Xu, Mechanism of thrombocytopenia in COVID-19 patients, Ann. Hematol. (2020), https://doi.org/10.1007/s00277-020-04019-0.
[25] F.A. Ruiz, C.R. Lea, E. Oldfield, R. Docampo, Human platelet dense granules contain polyphosphate and are similar to acidocalcisomes of bacteria and unicellular eukaryotes, J. Biol. Chem. 279 (2004) 44250–44257.
[26] B. Lorenz, H.C. Schröder, Mammalian intestinal alkaline phosphatase acts as highly active exopolyphosphatase, Biochim. Biophys. Acta 1547 (2001) 254–261.
[27] X.H. Wang, M. Ackermann, E. Tolba, M. Neufurth, F. Wurm, Q. Feng, S. Wang, H.C. Schröder, W.E.G. Müller, Artificial cartilage bio-matrix formed of hyaluronic acid and Mg^{2+}-polyphosphate, Eur. Cell Mater. 32 (2016) 271–283.
[28] W.E.G. Müller, E. Tolba, H.C. Schröder, S. Wang, G. Glaßer, R. Muñoz-Espí, T. Link, X.H. Wang, A new polyphosphate calcium material with morphogenetic activity, Mater. Lett. 148 (2015) 163–166.
[29] I.I. Slowing, J.L. Vivero-Escoto, C.W. Wu, V.S. Lin, Mesoporous silica nanoparticles as controlled release drug delivery and gene transfection carriers, Adv. Drug Deliv. Rev. 60 (2008) 1278–1288.
[30] J.V. Fahy, B.F. Dickey, Airway mucus function and dysfunction, N. Engl. J. Med. 363 (2010) 2233–2247.
[31] W. Stöber, A. Fink, E. Bohn, Controlled growth of monodisperse silica spheres in the micron size range, Colloid Interface Sci. 26 (1968) 62–69.
[32] W. Vogelsberger, A. Seidel, G. Rudakoff, Solubility of silica gel in water, J. Chem. Soc./Faraday Trans. 88 (1992) 473–476.
[33] DAC/NRF [eds], Standardisierte Rezepturen, 5th Edition, Govi, Eschborn, 1997.
[34] W.E.G. Müller, M. Ackermann, S. Wang, M. Neufurth, R. Muñoz-Espí, Q. Feng, H.C. Schröder, X.H. Wang, Inorganic polyphosphate induces accelerated tube formation of HUVEC endothelial cells, Cell. Mol. Life Sci. 75 (2018) 21–32.
[35] K. Mori, M. Berreur, F. Blanchard, C. Chevalier, I. Guisle-Marsollier, M. Masson, F. Rédini, D. Heymann, Receptor activator of nuclear factor-kappaB ligand (RANKL) directly modulates the gene expression profile of RANK-positive Saos-2 human osteosarcoma cells, Oncol. Rep. 18 (2007) 1365–1371.
[36] M. Scimeca, S. Bischetti, H.K. Lamsira, R. Bonfiglio, E. Bonanno, Energy dispersive X-ray (EDX) microanalysis: A powerful tool in biomedical research and diagnosis, Eur. J. Histochem. 62 (2018) 2841.
[37] R.H. Lyles, C. Poindexter, A. Evans, M. Brown, C.R. Cooper, Nonlinear model-based estimates of IC(50) for studies involving continuous therapeutic dose-response data, Contemp. Clin. Trials 29 (2008) 878–886.
[38] S.A. Ali, M.I. Hassan, A. Islam, F. Ahmad, A review of methods available to estimate solvent-accessible surface areas of soluble proteins in the folded and unfolded states, Curr. Protein Pept. Sci. 15 (2014) 456–476.
[39] V.L. Mendoza, R.W. Vachet, Probing protein structure by amino acid-specific covalent labeling and mass spectrometry, Mass Spectrom. Rev. 28 (2009) 785–815.
[40] J.L. Millán, M.P. Whyte, L.V. Avioli, W.H. Fishman, Hypophosphatasia (adult form): quantitation of serum alkaline phosphatase isoenzyme activity in a large kindred, Clin. Chem. 26 (1980) 840–845.
[41] X.K. Ma, N.H. Lee, H.J. Oh, J.W. Kim, C.K. Rhee, K.S. Park, S.J. Kim, Surface modification and characterization of highly dispersed silica nanoparticles by a cationic surfactant, Colloids Surfaces A Physicochemical and Engineering Aspects 358 (2010) 172–176.
[42] G. Asab, E.A. Zereffa, T.A. Seghne, Synthesis of silica-coated Fe3O4 nanoparticles by microemulsion method: Characterization and evaluation of antimicrobial activity, Intern. J. Biomat. (2020 (2020)) ID 4783612.
[43] L.Y. Geer, M. Domrachev, D.J. Lipman, S.H. Bryant, CDART: protein homology by domain architecture, Genome Res. 12 (2002) 1619–1623.
[44] A.W. Ng, A. Bidani, T.A. Heming, Innate host defense of the lung: effects of lung-lining fluid pH, Lung 182 (2004) 297–317.
[45] C.R. Bodem, L.M. Lampton, D.P. Miller, E.F. Tarka, E.D. Everett, Endobronchial pH. Relevance of aminoglycoside activity in gram-negative bacillary pneumonia, Am. Rev. Respir. Dis. 127 (1983) 39–41.
[46] H. Engelberg, Plasma heparin levels in normal man, Circulation 23 (1961) 578–581.
[47] P. Carlsson, L. Kjellén, Heparin biosynthesis, Handb. Exp. Pharmacol. 207 (2012) 23–41.
[48] S.K. Kritas, G. Ronconi, A. Caraffa, C.E. Gallenga, R. Ross, P. Conti, Mast cells contribute to coronavirus-induced inflammation: new anti-inflammatory strategy, J. Biol. Regul. Homeost, Agents 34 (1) (2020), https://doi.org/10.23812/20-Editorial-Kritas.
[49] N. Tang, H. Bai, X. Chen, J. Gong, D. Li, Z. Sun, Anticoagulant treatment is associated with decreased mortality in severe coronavirus disease 2019 patients with coagulopathy, J. Thromb. Haemost. 18 (2020) (2019) 1094–1099.
[50] D.G. Drescher, S. Dakshnamurthy, M.J. Drescher, N.A. Ramakrishnan, Surface plasmon resonance (SPR) analysis of binding interactions of inner-ear proteins, Methods Mol. Biol. 1427 (2016) 165–187.
[51] A.S. Woods, S. Ferré, Amazing stability of the arginine-phosphate electrostatic interaction, J. Proteome Res. 4 (2005) 1397–1402.
[52] A.S. Woods, J.M. Koomen, B.T. Ruotolo, K.J. Gillig, D.H. Russel, K. Fuhrer, M. Gonin, T.F. Egan, J.A. Schultz, A study of peptide-peptide interactions using MALDI ion mobility o-TOF and ESI mass spectrometry, J. Am. Soc. Mass Spectrom. 13 (2002) 166–169.
[53] A.S. Woods, The mighty arginine, the stable quaternary amines, the powerful aromatics, and the aggressive phosphate: their role in the noncovalent minuet, J. Proteome Res. 3 (2004) 478–484.
[54] L. Patthy, E.L. Smith, Reversible modification of arginine residues. Application to sequence studies by restriction of tryptic hydrolysis to lysine residues, J. Biol. Chem. 250 (1975) 557–564.
[55] Y. Itoh, Y. Nakashima, S. Tsukamoto, T. Kurohara, M. Suzuki, Y. Sakae, M. Oda, Y. Okamoto, T. Suzuki, N^{+}-C-H···O Hydrogen bonds in protein-ligand complexes, Sci. Rep. 9 (2019) 767.
[56] I.S. Kulaev, V.M. Vagabov, T.V. Kulakovskaya, The Biochemistry of Inorganic Polyphosphates, Wiley, Chichester, 2004.
[57] R.H. Ellinger, Phosphates as food ingredients, CRC Press, Boca Raton, 2018, p. 52.
[58] B. Nami, A. Ghanaeian, K. Ghanaeian, N. Nami, The effect of ACE2 inhibitor MLN-4760 on the interaction of SARS-CoV-2 spike protein with human ACE2: a molecular dynamics study, ChemRxiv (2020), https://doi.org/10.26434/chemrxiv.12159945.v1.

[59] B.M. Luttrell, The biological relevance of the binding of calcium ions by inositol phosphates, J. Biol. Chem. 268 (1993) 1521–1524.
[60] P. Bünning, J.F. Riordan, The functional role of zinc in angiotensin converting enzyme: implications for the enzyme mechanism, J. Inorg. Biochem. 24 (1985) 183–198.
[61] I.Y. Kim, E. Joachim, H. Choi, K. Kim, Toxicity of silica nanoparticles depends on size, dose, and cell type, Nanomedicine 11 (2015) 1407–1416.
[62] M. Koupenova, H.A. Corkrey, O. Vitseva, G. Manni, C.J. Pang, L. Clancy, C. Yao, J. Rade, D. Levy, J.P. Wang, R.W. Finberg, E.A. Kurt-Jones, J.E. Freedman, The role of platelets in mediating a response to human influenza infection, Nat. Commun. 10 (2019) 1780.
[63] M. Koupenova, O. Vitseva, C.R. MacKay, L.M. Beaulieu, E.J. Benjamin, E. Mick, E.A. Kurt-Jones, K. Ravid, J.E. Freedman, Platelet-TLR7 mediates host survival and platelet count during viral infection in the absence of platelet-dependent thrombosis, Blood 124 (2014) 791–802.